Fast Distance Protection Scheme for Wind Farm Transmission Lines Considering R-L and Bergeron Models

Zepeng Hu, Bin Li, Yuping Zheng, Tonghua Wu, Jiawei He, Bin Yao, Yaru Sheng, Wei Dai, and Xindong Li

***Abstract*—The distributed capacitance of the line becomes larger as the scale of wind farms, the transmission voltage level, and the transmission distance increase. Hence, the error of the traditional time-domain distance protection scheme based on the R-L model, which ignores the distributed capacitance of the line, becomes unacceptable. Therefore, the error of the time-domain fault location method based on the R-L model, especially the maximum error range, is theoretically analyzed in this paper. On this basis, a novel fault location method based on the R-L and Bergeron models is proposed. Then, a fast time-domain distance protection scheme is designed. In the proposed scheme, the error in the fitting calculation is used to construct a weight matrix, and an algorithm for solving the time-domain differential equations is designed to improve the calculation speed and stability. Compared with the traditional frequency-domain distance protection scheme, the proposed scheme is independent of the power supply characteristics; thus, it is suitable for wind farm transmission lines. In addition, compared with the traditional method based on the R-L model, the proposed scheme effectively avoids the negative influence of the distributed capacitance of the line, which significantly improves the operating speed. Different types of faults are simulated by PSCAD/EMTDC to verify the effectiveness and superiority of the proposed scheme.**

***Index Terms*—Transmission line, R-L model, time-domain distance protection, wind farm.**

I. Introduction

In response to issues such as global climate change, environmental pollution, and energy strategies, countries around the world are actively promoting the low-carbon, clean, and sustainable transformation of energy systems [1], [2]. For example, China is proposing to achieve an "carbon emission peak" by 2030 and "carbon neutrality" by 2060. At the 2020 Climate Ambition Summit, China proposed a development goal of achieving a total capacity of wind power and photovoltaics exceeding 1200 GW by 2030. Therefore, it is extremely important to ensure the safe and reliable operation of a power system integrated with a high proportion of renewable energy power generation.

At present, wind power generation is one of the most typical types of renewable energy power generation. However, the operation mode of a wind farm is obviously random and intermittent owing to the effects of climatic conditions and other factors [3]-[5]. In addition, the fault response characteristics of wind power generators, e. g., doubly-fed induction generators (DFIGs), are quite different from those of conventional synchronous generators [6]-[8]. Obviously, the above factors will profoundly affect the performance of conventional protection schemes [9]-[12].

Recently, much of the literature has focused on protection schemes that consider the effects of integrated wind farms [13]-[32]. In this paper, distance protection for transmission lines is mainly discussed; thus, research on improving the performance of distance protection is introduced below. On the basis of the ratio of the current and voltage on the wind farm side and information related to the wind turbines participating in power generation, an adaptive method for setting wind-farm-side distance protection is proposed in [18]. A modified permissive overreach transfer trip scheme and a fault current classification technique are devised in [19] to address the incorrect measurement of the impedance of the distance relay. In [20], the operation characteristics for distance protection when a wind farm is integrated are analyzed considering the variations in the load, voltage, impedance, and frequency. Then, a method that adaptively sets the protection boundary using only local information is proposed. An adaptive unit that adjusts the relay trip characteristic based on an artificial neural network is designed in [21] to cope with changes in the operation mode of the wind farm. An adaptive distance protection scheme based on frequency spectrum analyses of the current and voltage on both sides of the line after a fault occurs is proposed in [22].

Manuscript received: June 29, 2021; revised: November 8, 2021; accepted: March 22, 2022. Date of CrossCheck: March 22, 2022. Date of online publication: May 26, 2022.

This work was supported by the Science and Technology Program of State Grid Corporation of China "Research on the Principle of Fast Protection in Time-frequency Domain with Single-ended Quantities of High-proportion New Energy Grid Lines" (No. 5100-202040327A-0-0-00).

Z. Hu, B. Li (corresponding author), J. He, B. Yao, and Y. Sheng are with the Electrical Engineering and Automation, Tianjin University, Tianjin, China (e-mail: hzp_cqu@tju. edu. cn; libin_tju@126. com; hejiawei_tju@126. com; yaobin@tjuer.com; shengyaru_tju@126.com).

Y. Zheng, T. Wu, W. Dai, and X. Li are with the State Key Laboratory of Smart Grid Protection and Control, NARI Group Corporation, Nanjing, China (e-mail: zhengyuping@sgepri.sgcc.com.cn; wutonghua@sgepri.sgcc.com.cn; daiwei@sgepri.sgcc.com.cn; lixindong@sgepri.sgcc.com.cn)

DOI: 10.35833/MPCE.2021.000423

However, it is noted that the above studies are mostly based on frequency-domain information. According to the response characteristic of a DFIG after a fault, the fault current of a power system integrated with a wind farm may exhibit frequency deviations and contain high-frequency harmonics [23]. This means that it is difficult to accurately extract the power frequency signal during the initial stage of a fault; thus, the above-mentioned protection schemes cannot operate during this initial stage [24]-[27].

Reference [28] points out that the algorithm for solving differential equations is not affected by the frequency in principle by analyzing the influence of the frequency offset on the distance protection based on the power frequency. Therefore, the time-domain distance protection based on a lumped parameter model is widely studied. In [29], an algorithm for solving differential equations, which combines fault iteration, digital low-pass filtering, and fault point voltage reconstruction, is proposed. In [30], a distance protection scheme that has a strong ability to mitigate transient overreach using an error correction of a time-domain equation model is proposed. In [31], a novel solution based on an algorithm that solves the differential equations of the R-L model under zero-voltage fault conditions is proposed. The above-mentioned schemes for time-domain distance protection do not consider the influence of the distributed capacitance of a transmission line. As the length of the transmission line increases, the error caused by ignoring the distributed capacitance becomes larger and cannot be ignored anymore. In [32], a time-domain distance protection scheme for a long-distance transmission line integrated with a wind farm is proposed, which calculates the fault distance between a set point and the fault point using the Bergeron model to determine whether the protection is active. However, when the Bergeron model is directly used to calculate the fault distance, it may cause the calculated target point to exceed the fault point. Under this condition, the calculated voltage and current are no longer true, especially when the transition resistance is large. Obviously, this will result in incorrect operation of the protection.

Therefore, a novel fast time-domain distance protection scheme based on iteration of the Bergeron model and error correction of the weight matrix is proposed in this paper. After a fault, the distance to the fault point is first estimated by an improved fault location algorithm based on the R-L model. Then, a confidence interval for the calculated value is evaluated according to a theoretical analysis of the steady-state and transient errors. According to this confidence interval, a point between the protection position and the fault point is selected. Moreover, the voltage and current at the selected point are calculated using the Bergeron model. Next, the voltage and current at the selected point are used to recalculate the fault distance with the improved fault location algorithm based on the R-L model. The above processes are iterated so that the selected point gradually approaches the fault point more closely without crossing the point of failure. Moreover, the effect of the distributed capacitance is also eliminated. After the iteration process, the final calculated result is obtained, and a protection judgment is made. The major contributions of this paper are summarized as follows.

1) The theoretical error of the fault location method based on the R-L model is derived in this paper. Hence, the limitations of the traditional time-domain distance protection scheme based on the R-L model and its applicable scenarios are clarified.

2) On the basis of the above error analysis, an iterative scheme combing the Bergeron and R-L models is proposed. The proposed scheme eliminates the location error caused by ignoring the distributed capacitance in the R-L model.

3) A stability enhancement algorithm based on the error weight matrix and the removal of singular points is proposed. Compared with existing time-domain distance protection schemes, the proposed algorithm has a faster convergence speed, greater stability, and better robustness to the transition resistance and noise. The feasibility and superiority of the proposed algorithm are verified by many simulation cases.

The remainder of this paper is organized as follows. Section II presents the time-domain distance protection scheme based on the R-L model and a theoretical derivation of its error range. In Section III, we introduce the principles of the proposed fast time-domain distance protection scheme. A case analysis and comparison are discussed in Section IV. Finally, Section V concludes the paper.

II. Time-domain Distance Protection Scheme Based on R-L Model and Theoretical Derivation of Its Error Range

With the rapid growth of wind power, the demand for long-distance and large-scale power transmission is increasing. Therefore, the error caused by ignoring the distributed capacitance of the transmission line in the R-L model may adversely affect protection. In view of this problem, the values of the errors in the distributed capacitance and its maximum range are analyzed in this section.

A. Time-domain Differential Equations

The differential equations for time-domain distance protection are based on the transmission line model with lumped parameters. The transmission line from the protection position to the fault point is represented by the series connection of resistors and inductors, i.e., equivalent to the R-L model. As shown in Fig. 1, a single-phase grounding fault occurs at point F on the transmission line; a distance protection is located at the position p; r_1 and l_1 are the resistance and inductance per unit length of the transmission line, respectively; R_F is the transition resistance; i_F is the current flowing through the transition resistance; i_m and u_m are the current and voltage at the position p, respectively; l is the total length of the transmission line; and x is the fault distance.

In the case of a phase A grounding fault, the voltage $u_{mA}(t)$ and current $i_{mA}(t)$ measured at the protection position are [29]-[32]:

$$u_{mA}(t)=[(i_{mA}(t)+3k_r i_0(t))r_1+l_1\mathrm{d}(i_{mA}(t)+3k_l i_0(t))/\mathrm{d}t]x+i_F(t)R_F \quad (1)$$

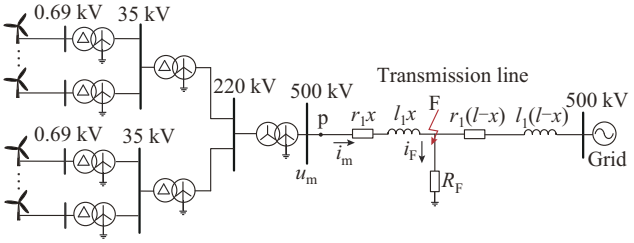

Fig. 1. R-L series model of a transmission line.

where $i_0(t)$ is the zero-sequence current; and $k_r=(r_0-r_1)/(3r_1)$ and $k_l=(l_0-l_1)/(3l_1)$ are the zero-sequence compensation coefficients of the resistance and inductance, respectively, and r_0 and l_0 are the zero-sequence resistance and inductance per unit length of the transmission line, respectively.

Under certain conditions, it is approximately assumed that the phase of the zero-sequence current flowing through the transition resistance is close to the phase measured at the protection position for single-phase grounding faults [33]. That is, $i_F=i_0/C_F$, where C_F is the zero-sequence shunt coefficient at the protection position. Using the median difference instead of the differential for discrete sampling data, (1) can be equivalent to:

$$u_{mA}(n)=[(i_{mA}(n)+3k_ri_0(n))r_1+(i_{mA}(n+1)+3k_ri_0(n+1)-i_{mA}(n-1)-3k_li_0(n-1))l_1/(2\Delta t)]x+i_0(n)R'_F \tag{2}$$

where n is the number of sampling sequences; Δt is the sampling interval; and $R'_F=R_F/C_F$.

Using the voltage and current continuously sampled by the protection, a series of equations such as (2) can be obtained and organized into matrix form as:

$$\boldsymbol{U}=\boldsymbol{I}\boldsymbol{\beta} \tag{3}$$

where $\boldsymbol{U}$, $\boldsymbol{I}$, and $\boldsymbol{\beta}$ are the voltage, current, and coefficient matrices, respectively, which can be calculated as:

$$\boldsymbol{U}=[u_{mA}(n-k+1)\quad u_{mA}(n-k+2)\quad ...\quad u_{mA}(n)]^T \tag{4}$$

$$\boldsymbol{I}=\begin{bmatrix} p(n-k+1) & p(n-k+2) & ... & p(n) \\ p_d(n-k+1) & p_d(n-k+2) & ... & p_d(n)\end{bmatrix}^T \tag{5}$$

$$\boldsymbol{\beta}=[x\quad R'_F]^T \tag{6}$$

where k is the number of sampling points in a data window for calculation; $p(n)$ is the current sampling sequence for calculation, which can be expressed as (7); and $p_d(n)$ is the differential derivative sequence of the current sampling points for calculation, which can be expressed as (8).

$$p(n)=i_{mA}(n)+3k_ri_0(n) \tag{7}$$

$$p_d(n)=(i_{mA}(n+1)+3k_li_0(n+1)-i_{mA}(n-1)-3k_li_0(n-1))/(2\Delta t) \tag{8}$$

On the basis of the sampling sequence of a certain redundant data window, the least-squares method is used to estimate and solve (3), i.e., fitting the coefficient matrix $\boldsymbol{\beta}$ so that the calculated value of the voltage matrix in the data window ($\boldsymbol{I\beta}$) and the actual value ($\boldsymbol{U}$) have the minimum distance in Euclidean space E, which can be expressed as:

$$E^2=\left\|\boldsymbol{U}-\boldsymbol{I\beta}\right\|_2^2 \tag{9}$$

By computing the partial derivative of the coefficient matrix $\boldsymbol{\beta}$ in the above expression and setting the partial derivative to be zero, $\boldsymbol{\beta}$ can be expressed as:

$$\boldsymbol{\beta}=(\boldsymbol{I}^T\boldsymbol{I})^{-1}\boldsymbol{I}^T\boldsymbol{U} \tag{10}$$

As aforementioned, the time-domain differential equations are constructed based on the R-L model for fitting and solving, and thus obtaining the fault distance, which is referred to as the R-L algorithm.

B. Error Caused by Distributed Capacitance and Its Influence on Distance Protection

1) Metallic Grounding Fault

By comparing the R-L model and the long line equation, the error in the fault distance calculation caused by ignoring the distributed capacitance in the R-L model is analyzed in this paper.

Taking a single-phase system as example, $\dot{U}_m$ and $\dot{I}_m$ are the voltage and current at the protection position, respectively. Then, the voltage of point x can be calculated using the voltage and current at the protection position and the long line equation as:

$$\dot{U}(x)=\dot{U}_m\cosh(\gamma x)-\dot{I}_mZ_c\sinh(\gamma x) \tag{11}$$

where γ is the propagation coefficient; and Z_c is the wave impedance of the transmission line.

When a metallic grounding fault occurs on the line, the voltage of the fault point is zero, i.e., $\dot{U}(x)=0$. Using (11), a relation between the measured impedance and the fault distance is obtained in (12). The measured impedance accounts for the distributed capacitance of the transmission line.

$$Z_m(\omega,x)=Z_c\sinh(\gamma x)/\cosh(\gamma x) \tag{12}$$

where ω is the power frequency.

When the transmission line is equivalent to that in the R-L model, the unit impedance of the line is $r_1+j\omega l_1$. Using the more accurate measured impedance in (12), the fault distance calculated with the R-L model can be expressed as:

$$x_{CALC}=\left|Z_m(\omega,x)/(r_1+j\omega l_1)\right| \tag{13}$$

At this point, the true fault distance is x; thus, the error in the fault distance calculation caused by ignoring the distributed capacitance of the line can be expressed as:

$$E_c(\omega,x)=x_{CALC}-x \tag{14}$$

For a transmission line with a total length of l_h and a protection setting coefficient of k_z, the fault location error at x must be less than $\left|k_zl_h-x\right|$ if the fault occurs at x on the line. The calculated fault distance can correctly fall in or out of the protection zone only in this manner. Therefore, the condition for correct operation of distance protection is that the fault location error is not greater than the difference between the fault distance and the set distance. The allowable error of the calculated fault distance can be expressed as:

$$E_a(l_h,x)=\left|k_zl_h-x\right| \tag{15}$$

It can be observed from (9) that the error caused by the distributed capacitance in the R-L model is related to the frequency. The access of a wind farm may add an attenuation

current component of the rotor speed frequency to the fault current, and its frequency is 0.7-1.3 times the power frequency [34], [35], i.e., 35-65 Hz.

Given the transmission line parameters $r_1=0.208$ Ω/km, $l_1=0.8984$ mH/km, and $c_1=0.0129$ μF/km, the error caused by the distributed capacitance at 35, 50, and 65 Hz is calculated. Taking the distance protection setting value of 90% as an example, the allowable error for distance protection is calculated when the line length is 200, 300, and 400 km, respectively. The calculated results are shown in Fig. 2(a). From Fig. 2(a), it is found that the calculated results for the error are positive when the R-L model ignores the distributed capacitance. Therefore, the distance protection may refuse to operate when the fault point is close to the set point. The abscissa of the intersection of the error curve of the R-L model $E_c(\omega,x)$ and the allowable error curve of the distance protection $E_a(l_h,x)$ in Fig. 2(a) is the starting point at which distance protection may refuse to operate. Figure 2(b) shows the possible rejection lengths of protection for different line lengths and frequencies.

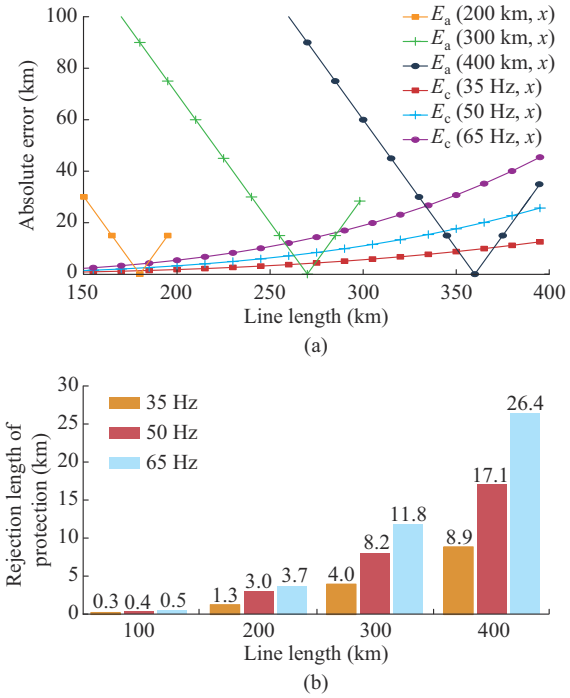

Fig. 2. Error of R-L model at different frequencies and its influence on distance protection. (a) Ranges of error in R-L model and allowable error of distance protection. (b) Rejection lengths of protection for different line lengths and frequencies.

The above analysis of the possible rejection length of protection is based on the steady state. In fact, owing to the access of the large-scale wind farm, the error in the calculated fault distance will be further increased as the high-frequency component in the fault transient increases. The reliability of distance protection will be reduced further.

2) Influence of Transition Resistance on Error in Distributed Capacitance

When a fault with a transition resistance occurs at x on the line, the voltage at the fault point is no longer zero, and the assumption that $\dot{U}(x)=0$ in the aforementioned error analysis is no longer valid.

At $x=0$, we expand the long line equation in (11) by a first-order Taylor expansion:

$$\dot{U}(x)=\dot{U}_m-(r_1+j\omega l_1)\dot{I}_m x+R_2(x) \tag{16}$$

where $R_2(x)=\dot{U}(\xi_x)\gamma^2x^2/2\,(0<\xi_x<x)$, which is the Lagrange remainder of the first-order Taylor expansion in (16), and ξ_x is a certain point from the protection position to the fault point.

It is noted that when (16) ignores the Lagrange remainder and is transformed into the time domain, it becomes a time-domain R-L equation. Therefore, $R_2(x)$ is the error of the R-L model.

In the case of a fault with a transition resistance, the fault distance can be calculated as:

$$x_{CALC}=\left|(\dot{U}_m-\dot{U}(x)+R_2(x))/[(r_1+j\omega l_1)\dot{I}_m]\right|\le x_{CALC(1)}+x_{CALC(2)} \tag{17}$$

where $x_{CALC(1)}=\left|(\dot{U}_m-\dot{U}(x))/[(r_1+j\omega l_1)\dot{I}_m]\right|$; and $x_{CALC(2)}=\left|R_2(x)/[(r_1+j\omega l_1)\dot{I}_m]\right|$. Therefore, $x_{CALC}-x_{CALC(1)}\le x_{CALC(2)}$.

$x_{CALC(1)}$ can be regarded as the fault distance calculated by the R-L model in the physical sense, and $x_{CALC(2)}$ is the calculated fault distance of the Lagrange remainder. Therefore, the error in the fault distance calculated by the R-L model cannot exceed $x_{CALC(2)}$ at most. Since an accurate value for $|\dot{U}(\xi_x)|$ in $R_2(x)$ cannot be determined, an accurate calculated value for $x_{CALC(2)}$ cannot be obtained. However, from the derivation process for the Lagrange remainder, it is known that $|\dot{U}(\xi_x)|$ is the voltage at a certain point from the protection position to the fault point; thus, it satisfies the condition that $|\dot{U}(\xi_x)|<|\dot{U}_m|$. Therefore, the range of $x_{CALC(2)}$ can be expressed as:

$$\begin{aligned}x_{CALC(2)}&=\left|(g_1+j\omega c_1)\dot{U}(\xi_x)x^2/(2\dot{I}_m)\right|<\\&\left|(g_1+j\omega c_1)\dot{U}_m x^2/(2\dot{I}_m)\right|\approx\left|j\omega c_1 Z_m x^2/2\right|\end{aligned} \tag{18}$$

where g_1 is the conductance per unit length of the transmission line; and Z_m is the apparent impedance at the protection position. Assuming that a transmission line is equivalent to the Γ model, Z_m can be expressed as:

$$Z_m=[(r_1+j\omega l_1)x+R_F]\,//\,[1/(j\omega c_1 x)] \tag{19}$$

By substituting (19) into (18) and rearranging, the maximum error is expressed as:

$$E_{c,max}(\omega,x,R_F)=\left|\frac{YWx^3+WR_Fx^2}{2(1+YWx^2+WR_Fx)}\right| \tag{20}$$

where $Y=r_1+j\omega l_1$; and $W=j\omega c_1$.

When the frequency is set to be 50 Hz, the rejection length of protection caused by the error in the distributed capacitance is calculated for different transition resistances, as shown in Fig. 3. By comparing Fig. 3 and Fig. 2(b), the difference between the rejection length of protection calculated by the accurate error and that calculated by the maximum error is small in the case of metal grounding. This indicates that the scaling of the error range in this section is reasonable.

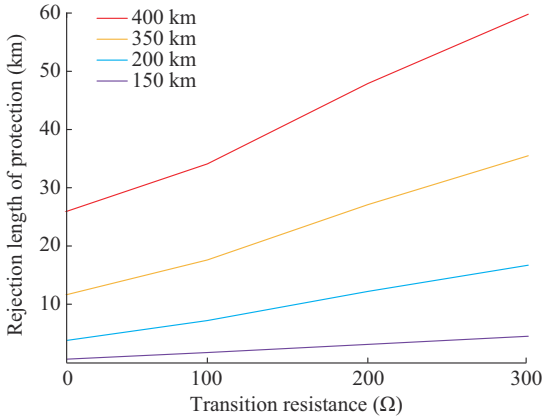

Fig. 3. Rejection lengths of protection for different transition resistances and line lengths.

III. Principles of Fast Time-domain Distance Protection Scheme

A. Improved Algorithm for Solving Differential Equations of R-L Model

In this subsection, an improvement to the algorithm for solving the differential equations of the R-L model based on the error weight matrix is presented (referred to as improved R-L algorithm). This algorithm can improve the convergence speed while ensuring stability. The calculated transient error based on the fitting error is analyzed.

1) Removal of Singular Points

When solving the differential equations of the R-L model, the difference instead of the differentiation for derivation causes algorithm errors. Differential derivation has the largest error across the sampling point at the peak of the current. Defining these points as singular points, it is easy to show that these points satisfy:

$$p_{\mathrm{d}}(n)p_{\mathrm{d}}(n-1)<0 \tag{21}$$

As the protection installation continuously acquires sampling data, the current derivative sequence $p_{\mathrm{d}}(n)$ is continuously determined and detected by (21). If sampling point n_{s} meets the above condition, the fitting calculation weight of n_{s} and its nearby points will be reduced. To this end, a diagonal matrix of error weights $\boldsymbol{W}_{\mathrm{I}}=\mathrm{diag}(W_{\mathrm{I}}(n))$ is introduced, whose element is:

$$W_{\mathrm{I}}(n)=\begin{cases}1/k & n=n_{\mathrm{s}}\pm c_{\mathrm{n}}\\ 1 & n\neq n_{\mathrm{s}}\pm c_{\mathrm{n}}\end{cases} \tag{22}$$

where k is the number of sampling points in the unit data window; and c_{n} is the value of the real number, which is determined by the number of sampling points in the unit data window.

After introducing the matrix of error weights, (9) can be rewritten as:

$$E^2=(\boldsymbol{U}-\boldsymbol{I}\boldsymbol{\beta})^{\mathrm{T}}\boldsymbol{W}_{\mathrm{I}}(\boldsymbol{U}-\boldsymbol{I}\boldsymbol{\beta}) \tag{23}$$

By solving the equation above, the coefficient matrix to be calculated after the weights of the singular points are reduced is obtained as:

$$\boldsymbol{\beta}=(\boldsymbol{I}^{\mathrm{T}}\boldsymbol{W}_{\mathrm{I}}\boldsymbol{I})^{-1}\boldsymbol{I}^{\mathrm{T}}\boldsymbol{W}_{\mathrm{I}}\boldsymbol{U} \tag{24}$$

2) Stability Enhancement

In general, the calculated results may have relatively large fluctuations for the same sampling rate when the data window for calculating the differential equations is short; when the data window is relatively long, the calculated results are more stable. However, during the process of the transient-state to steady-state calculation, the long data window may contain both transient- and steady-state data, resulting in the calculated results that reach the final steady-state value more slowly than the shorter data window.

In order to solve the problems above, a short sliding data window is selected for calculation in this paper to ensure rapid convergence. After the calculation starts to enter the steady state, a matrix of error weights is introduced to calculate the weighted average of the fitting results to ensure the stability of the calculation. The error weight matrix is determined as follows.

The fitting error in the unit data window is defined as:

$$E_{\mathrm{r}}=\sum_{i=n-k+1}^{n}\sqrt{[(\boldsymbol{U}(i)-\boldsymbol{I}(i)\boldsymbol{\beta})/\boldsymbol{U}(i)]^2}\Big/(k-2) \tag{25}$$

The value of the fitting error reflects the degree of agreement between the results of the fitting calculation and the true parameters. When the transient process is severe, the differential equations cannot obtain stable solutions, and the fitting error is relatively large. When the calculation begins to enter the steady state, the fitting error approximates zero. Therefore, the reciprocal of the fitting error $1/E_{\mathrm{r}}$ can be used as the weight coefficient of the result of a single fitting calculation. A larger weight coefficient means that the result of the fitting calculation is closer to the actual value. In this paper, a specific value of E_{r} is used as the threshold for determining whether the calculation starts to enter the steady state. When E_{r} is larger than the threshold, the calculated results will not be artificially modified.

When E_{r} is less than the threshold for the first time, the previous results of the fitting calculation are discarded. The subsequent calculated results are weighted and averaged according to the above-mentioned weight coefficients. Assume that E_{r} is less than the threshold for the first time at the m^{th} fitting calculation, and the $(m+z)^{\mathrm{th}}$ fitting calculation is currently in progress. The calculated result for the i^{th} fault location calculation is expressed as:

$$x_i=\begin{cases}x_i & i<m\\ \boldsymbol{X}\boldsymbol{E}_{\mathrm{r}}\Big/\sum_{i_{\mathrm{e}}=1}^{z}E_{\mathrm{r}}(i_{\mathrm{e}}) & i\geq m\end{cases} \tag{26}$$

where $E_{\mathrm{r}}(i_{\mathrm{e}})$ is the $i_{\mathrm{e}}^{\mathrm{th}}$ element of $\boldsymbol{E}_{\mathrm{r}}$; $\boldsymbol{X}=[x_m,x_{m+1},\ldots,x_{m+z}]$; and $\boldsymbol{E}_{\mathrm{r}}=[1/E_{\mathrm{r}(m)},1/E_{\mathrm{r}(m+1)},\ldots,1/E_{\mathrm{r}(m+z)}]^{\mathrm{T}}$, and $E_{\mathrm{r}(m)}$ is the fitting error at the m^{th} fitting calculation.

3) Transient Error

On the basis of a simulation analysis of a power grid with 100% integration of a wind farm, a single-phase grounding fault simulation experiment is carried out at intervals of 50 km on a 400 km line, and different transition resistances are set for each fault. The experimental data are calculated by a least-squares fitting based on the R-L model. The simulation model and calculation parameters are presented in Section

IV. The current threshold of the fitting error is set to be 1×10^{-5}. The time for the fitting error E_r to reach the threshold is defined as t_{thr}. The relative error of the transient calculation is defined as the ratio of the current calculated value minus steady-state value to the steady-state value.

In all examples, the value and distribution of t_{thr} are shown in Fig. 4(a), where the dots represent different examples, and the area of the ordinate reflects the aggregation degree of a large number of examples in the corresponding abscissa. The threshold value can be reached within 15 ms, and t_{thr} is concentrated in the range of 9-10 ms. The relative transient error ranges at t_{thr} and every 1 ms after t_{thr} are shown in Fig. 4(b), and they are taken as a basis of the protection scheme in this paper.

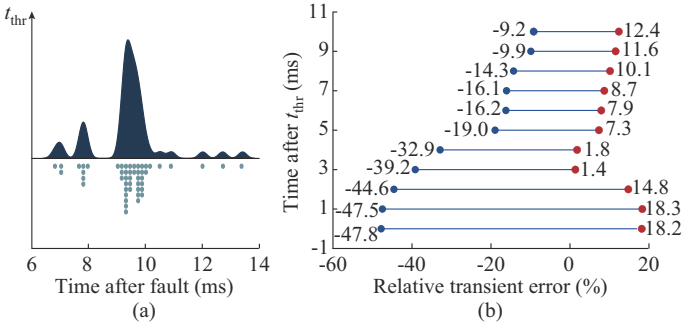

Fig. 4. Relationship between fitting error and transient error. (a) Time taken to reach fitting error threshold. (b) Relative transient error ranges at t_{thr} and every 1 ms after t_{thr}.

B. New Scheme for Distance Protection

1) Adopted Bergeron Model

In the time domain, the voltage and current at x on the transmission line can be calculated with the voltage and current at the protection position using the Bergeron model [36] as:

$$\begin{bmatrix} u_x(t) \\ i_x(t) \end{bmatrix} = \begin{bmatrix} A(x) & B(x) \\ C(x) & D(x) \end{bmatrix} \begin{bmatrix} u_m(t) \\ i_m(t) \end{bmatrix} \tag{27}$$

$$\begin{aligned} A(x)=-D(x)=D_e(\tau)[1/2+(r_1x)^2/(32z_c^2)+r_1x/(4z_c)]+\\ D_e(-\tau)[1/2+(r_1x)^2/(32z_c^2)-r_1x/(4z_c)]-(r_1x)^2/z_c^2 \end{aligned} \tag{28}$$

$$\begin{aligned} B(x)=-D_e(\tau)[3r_1x/8+3(r_1x)^2/(32z_c)+z_c/2+(r_1x)^3/128z_c^2]-\\ D_e(-\tau)[3r_1x/8-3(r_1x)^2/(32z_c)-z_c/2+\\ (r_1x)^3/(128z_c^2)]-r_1x/4+(r_1x)^3/(64z_c^2) \end{aligned} \tag{29}$$

$$\begin{aligned} C(x)=D_e(\tau)[1/(2z_c)+r_1x/(8z_c^2)]+D_e(-\tau)[-1/(2z_c)+\\ r_1x/(8z_c^2)]-r_1x/(4z_c^2) \end{aligned} \tag{30}$$

where $\tau=x/v$, v is the wave celerity; $D_e(\tau)$ is the retardation factor, so there is $f(t+\tau)=D_e(\tau)f(t)$; and $z_c=\sqrt{l_1/c_1}$ is the wave impedance of a nondissipative line.

When the R-L model is used for calculation, the error in the fault location caused by the distributed capacitance is $E_c(s,x)$. The voltage and current can be calculated from the protection position to x_α ($x_\alpha<x$) on the line by the Bergeron model in (27) and in combination with the phase-mode transformation. The R-L model is used to recalculate the fault distance using the voltage and current at x_α on the transmission line. The error in the fault distance caused by distributed capacitance in the final calculated result is $E_c(s,x)-E_c(s,x_\alpha)$. Therefore, the error caused by the distributed capacitance can be reduced through the calculation of the Bergeron model.

At the same time, the starting point of the R-L model is shifted towards the fault point because of the calculation of the Bergeron model. The influence of the distributed capacitance is reduced. Therefore, the convergence speed and stability of the calculation will be improved.

2) Iterative Calculation of Fault Distance

It can be observed from Section II that the fault location calculated by the R-L model is greater than the actual value when the error in the branching coefficient C_F is neglected. Further, it is more difficult to determine the true fault point owing to the effects of the transient process. If the voltage and current are calculated to the rear of the fault point by the Bergeron model, the obtained voltage and current are false. In particular, the phase of the calculated voltage is opposite to that of the actual value when a transition resistance exists. Therefore, the fault location based on this calculation will no longer be accurate. It is particularly important to select the appropriate calculation point for the Bergeron model. In this paper, a distance protection scheme based on Bergeron iteration combined with an error analysis is proposed. The flowchart of this scheme is shown in Fig. 5. Further explanation of Fig. 5 is as follows.

In each fault distance fitting calculation, the short sliding data window is selected, and the improved R-L algorithm is used for the fitting calculation. The value of the fault distance from the fitting calculation at t_{thr} is selected as x_0, and distance protection is first determined using (31). Considering the transient calculation error and the minimum error caused by the distributed capacitance, the fault distance can fall within the setting value, and the transition resistance is less than the setting value. Thus, the distance protection operates. When (31) is not satisfied at time t_{thr}, new calculated results for the fault distance are continuously obtained with the continuous entry of sampling data. From t_{thr} to 5 ms after t_{thr}, the distance protection determined by (31) is continued until it is satisfied.

$$[(x_n/(1+k^-)-E_c(x_n/(1+k^+))]<x_{set}\cap(R'_{F(n)}<R'_{F(set)})=1 \tag{31}$$

where x_{set} is the value set for the distance protection; $R'_{F(n)}$ is the calculated result for the equivalent transition resistance in the n^{th} fault location calculation; $R'_{F(set)}$ is the threshold value of the calculated transition resistance, which is obtained according to simulation, and a specific description and simulation data will be given later; and k^- and k^+ are the maximum negative and positive relative transient errors in the calculated value at the current moment, respectively. According to the previous analysis and considering the margin, the values of k^- of 0, 1, 2, 3, 4, and 5 ms after t_{thr} are taken to be –60%, –60%, –50%, –50%, –50%, and –25%, respectively; the values of k^+ of 0, 1, 2, 3, 4, and 5 ms after t_{thr} are taken to be 25%, 25%, 20%, 10%, 10%, and 10%, respectively.

When 5 ms after t_{thr} has passed, if (31) is still not satisfied, it can be determined that the fault point is closer to the set point or that the transition resistance is larger.

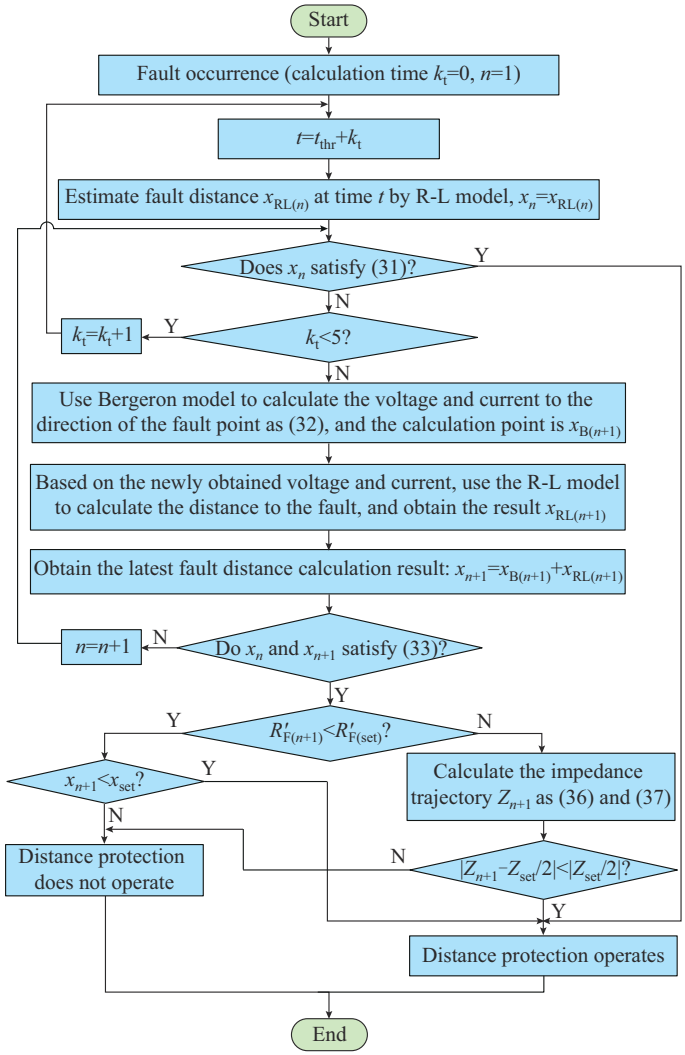

Fig. 5. Flowchart of distance protection scheme based on Bergeron iteration combined with error analysis.

Thus, the process of Bergeron iteration is started. The line length that can be calculated in the direction of the fault point by the Bergeron model is expressed in (32). The maximum error caused by the transient calculation and distributed capacitance is comprehensively considered to ensure that the calculation point is in front of the fault point. For single terminal information, it is impossible to know an accurate value for the transition resistance. In this paper, R_F is taken as the maximum possible value of the current voltage level when considering the maximum error of the distributed capacitance.

$$x_{B(n+1)}=x_{B(n)}+\min\{x_{RL(n)}/(1+k^+)-E_{c,\max}(x_{RL(n)}/(1+k^+)),\ x_{RL(n)}/(1+k^-)-E_{c,\max}(x_{RL(n)}/(1+k^-))\} \tag{32}$$

where $x_{B(n)}$ is the maximum distance that can be calculated with the Bergeron model during the n^{th} fault location calculation; $x_{RL(n)}$ is the n^{th} calculation result of fault distance based on the R-L model; k^+ is taken to be 10%; and $x_{B(1)}=0$.

The condition for stopping the iterative calculation of the Bergeron model is expressed in (33). This means that the error that is actually reduced by the two iterative calculations before and after is already less than the minimum theoretical error that can be reduced by the two iterative calculations. At this time, it is no longer an actual benefit to continue the iterative calculation. It is considered that the theoretical and transient calculation errors have been eliminated to the greatest extent.

$$\left|x_{n+1}-x_n\right|<k_b\left|E_c(x_{RL(n+1)})-E_c(x_{RL(n)})\right| \tag{33}$$

where k_b is the coefficient considering the error margin of the calculation, which is selected according to the calculation schedule, and is taken to be 1.2 in this study.

When the last two calculated results for the fault distance satisfy (33), the starting point of the calculation for the R-L model is already close to the fault point to the greatest extent. Thus, the transient calculation process has been greatly weakened. At this time, the margin of the transient calculation error is no longer considered. Therefore, the distance protection operation is judged by:

$$(x_n<x_{set})\cap(R'_{F(n)}<R'_{F(set)})=1 \tag{34}$$

In summary, when the transition resistance is less than the threshold value, the scheme combines the error in the distributed capacitance and the relative transient error of the improved algorithm to determine the distance protection. When the fault point is far from the set point and the error is not sufficiently high to cause the protection to refuse to operate or incorrectly operate, the scheme determines the distance protection operation. When the fault point is close to the set point, the voltage and current are gradually calculated to the front of the fault point by the iterative scheme on the premise of ensuring that the calculation point will not cross the fault point. This can eliminate the transient- and steady-state errors caused by the distributed capacitance to the maximum extent. On the basis of the above calculations, the final fault location is obtained to determine the distance protection.

3) Countermeasure for High-resistance Faults

When the transition resistance is large and the branch coefficient C_F can no longer be regarded as a real number, it is the most unfavorable situation for the R-L model. In this case, there may be a large error in the fault location. Therefore, the threshold is usually set for the calculated value of the transition resistance R'_F. However, when the threshold is set to be a small value, it may cause the protection to refuse to operate with the transition resistance fault in the protection zone. When the threshold is set to be a large value, it may cause the protection to operate incorrectly when the fault occurs outside the protection zone. For the R-L model, if the resistance and reactance are solved as two unknowns, as in (35), the impedance trajectory of the fault loop is calculated and compared with the setting impedance circle, and the fault zone can be better determined in the case of high-resistance faults, thus solving the above problems to a certain extent.

$$u_{mA}(t)=(i_{mA}(t)+3k_r i_0(t))R_x+L_x\mathrm{d}(i_{mA}(t)+3k_i i_0(t))/\mathrm{d}t+i_F(t)R'_F \tag{35}$$

where R_x and L_x are the lumped equivalent resistance and inductance of the fault loop, respectively.

However, the solution of (35) is not as stable as that of (1). The convergence speed is poor. Therefore, for the scheme proposed in this paper, the calculation for solving (35) is carried out after the Bergeron iteration is completed. This can greatly reduce the influence of the transient process on the calculated solution. Using the improved algorithm in this paper can make the calculated result more stable and converge faster. The final results for the impedance calculation can be expressed as:

$$\begin{cases} Z_{\mathrm{R}(n+1)} = x_{\mathrm{B}(n+1)} r_1 + R_{x(n+1)} \\ Z_{\mathrm{L}(n+1)} = \mathrm{j}\omega (x_{\mathrm{B}(n+1)} l_1 + L_{x(n+1)}) \end{cases} \tag{36}$$

where $Z_{\mathrm{R}(n+1)}$ and $Z_{\mathrm{L}(n+1)}$ are the equivalent impedance and inductive reactance of the fault loop during the $(n+1)^{\mathrm{th}}$ fault location calculation, respectively; and $R_{x(n+1)}$ and $L_{x(n+1)}$ are the equivalent resistance and inductance of the fault loop calculated by (35) with the voltage and current at $x_{\mathrm{B}(n+1)}$ on the line, respectively.

The value of the fault impedance calculated with (36) is compared with that of the setting impedance circle to determine the distance protection operation.

$$\left| Z_{n+1} - 1/(2Z_{\mathrm{set}}) \right| < 1 \Big/ \left| 2Z_{\mathrm{set}} \right| \tag{37}$$

where $Z_{n+1} = Z_{\mathrm{R}(n+1)} + Z_{\mathrm{L}(n+1)}$; and Z_{set} is the setting impedance of the distance protection. On the basis of the above improved algorithm and the simulation examples in the following section, $R'_{\mathrm{F(set)}}$ is set to be a smaller value of 300 Ω to prevent the protection from incorrect operation in the case of external faults.

IV. Case Analysis and Comparison

A. Simulation Model and Parameters

In PSCAD/EMTDC, the equivalent model for 100% integration of a wind farm into the power grid is built, as shown in Fig. 1. A total of 100 DFIGs of 5 MW are installed in the wind farm, which can provide 500 MW of electricity to the main grid. The detailed parameters of the DFIGs are listed in Table I. In the simulation setting, when a serious fault occurs, a crowbar is normally inserted, and the converter is blocked. The transmission voltage level is 500 kV, and the length of the transmission line is 400 km. The detailed parameters of the transmission line are listed in Table II.

TABLE I
Parameters of DFIGs

Parameter	Value
Rated power	5 MW
Number of DFIGs	100
Rated voltage	690 V
Rated stator frequency	50 Hz
Stator resistance	0.0054 p.u.
Stator leakage inductance	0.10 p.u.
Wound rotor inductance	0.00607 p.u.
Wound rotor leakage inductance	0.11 p.u.
Rated wind speed	10.5 m/s

TABLE II
Parameters of Transmission Line

Parameter	Value
Positive- or negative-sequence resistance	0.0208 Ω/km
Positive- or negative-sequence inductance	0.8984 mH/km
Positive- or negative-sequence capacitance	0.0129 μF/km
Zero-sequence resistance	0.1148 Ω/km
Zero-sequence inductance	2.2886 mH/km
Zero-sequence capacitance	0.0052 μF/km

B. Validation of Bergeron Model

In the analysis and calculation of the cases in this paper, the fault is set at the voltage peak at 3 s, the simulated sampling rate is 10 kHz, the sampled data are filtered through a 120 Hz Butterworth third-order low-pass filter, and the distance protection I segment is set to be 90% of the line length.

To verify the effectiveness of using the Bergeron model to reduce the steady-state error and transient process, a single-phase grounding metallic fault is set at 300 km on the transmission line. Using the Bergeron model in (27) and phase-to-mode transformation, the voltage and current at the protection position are calculated at 90, 180, and 270 km on the transmission line, respectively. The above Bergeron calculation points are used as the starting points of the R-L model to fit the fault distance. The calculation results of fault distance at different points by Bergeron model are shown in Fig. 6. After the calculation of the Bergeron model, a smaller error in the calculated results, faster convergence, and smaller fluctuations are obtained when the starting point of the R-L model calculation is closer to the fault point.

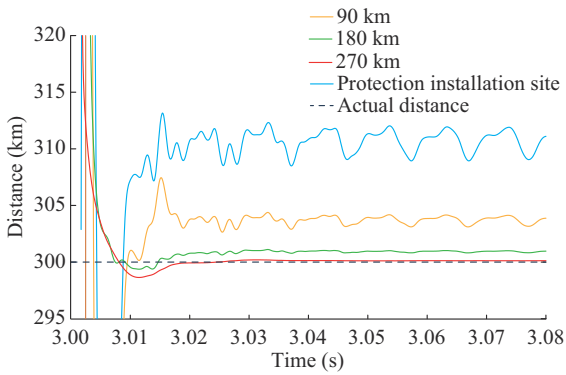

Fig. 6. Calculation results of fault distance at different points by Bergeron model.

C. Verification of Proposed Scheme

1) Verification of Proposed Improved R-L Algorithm for Improving Calculation Speed and Stability

When the fault points are far away from the protection setting point and the transition resistance is less than the threshold, it can be concluded that the error range meets the protection operation requirements in the proposed protection scheme. Thus, the Bergeron iteration will not be triggered. To verify the effectiveness of the improved R-L algorithm for solving the differential equations of the R-L model, a sin-

gle-phase metallic grounding fault is set at 100, 200, and 300 km on the transmission line. When performing least-squares fitting and solving, the data windows used for calculation are selected to be 0.8, 5, and 10 ms, respectively. The latter two are the length of the data windows commonly used in other papers when fitting and solving the differential equations of the R-L model [29]-[32]. The improved R-L algorithm proposed in this paper is based on the 0.8 ms short-term data window. The results of the fitting results for different fault distances and different data windows are shown in Fig. 7. The volatility of the improved R-L algorithm is smaller compared with the 5 ms data window. The improved R-L algorithm can converge to the vicinity of the calculated steady-state value faster than the 10 ms data window. The improved R-L algorithm considers the speed and stability of the fitting calculation.

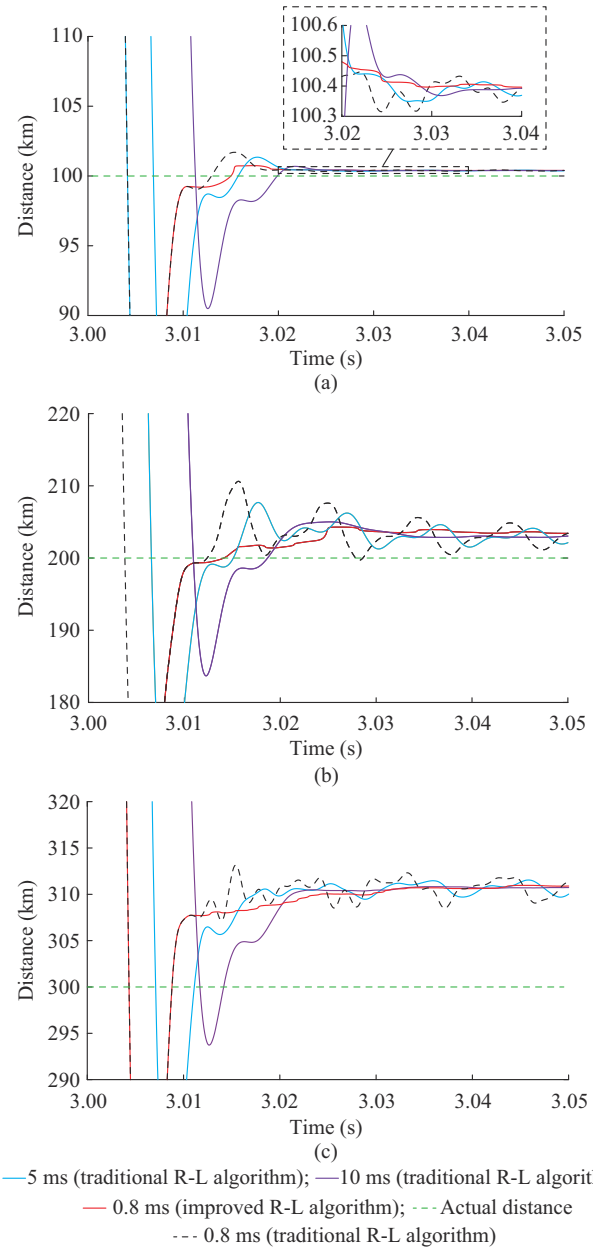

Fig. 7. Fitting results for different fault distances and different data windows. (a) 100 km. (b) 200 km. (c) 300 km.

2) Verification of Proposed Scheme for Eliminating Error

When the fault point is close to the setting point of distance protection, the proposed scheme triggers Bergeron iteration. To verify the effectiveness of the proposed scheme in reducing the transient- and steady-state errors, a single-phase metallic grounding fault is set at 342, 350, and 378 km on the transmission line, respectively.

The power frequency algorithm based on Fourier transform (referred to as Fourier algorithm), the traditional R-L algorithm, the improved R-L algorithm, and the proposed scheme are used to calculate the fault distance, respectively. The results are shown in Fig. 8.

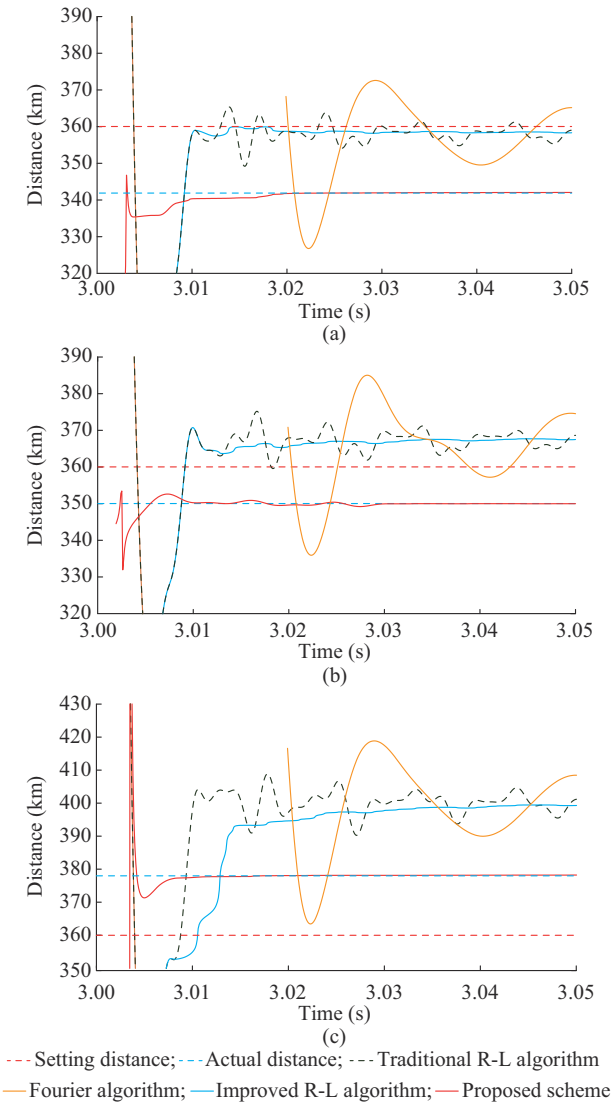

Fig. 8. Results of fitting calculation for fault distances when a single-phase metallic grounding fault is set at 342, 350, and 378 km on transmission line. (a) 342 km. (b) 350 km. (c) 378 km.

When the fault occurs at 95% of the protection setting value (342 km), the traditional R-L algorithm fluctuates up and down at this value, resulting in incorrect operation. The Fourier algorithm has the largest error and fluctuation. The improved R-L algorithm is stable below the setting value, and the proposed scheme converges near the actual value of the fault distance. In case of terminal fault in the protection

zone, the improved R-L algorithm and the proposed scheme can correctly operate. When the fault occurs at 350 km on the transmission line, the fault distance calculated by the traditional R-L algorithm completely exceeds the setting value because the distributed capacitance is ignored, or it exceeds the full length of the transmission line. The proposed scheme can quickly converge near the actual value of the fault distance, and the protection can correctly operate. When the fault occurs at 105% of the protection setting value (378 km), each algorithm can ensure that the protection does not malfunction, whereas the proposed scheme can obtain a more accurate and stable fault distance.

3) Effect of Transition Resistance and More Examples

To verify the anti-transition resistance capability of the proposed scheme, a single-phase grounding fault with a 300 Ω transition resistance is set at 300 and 378 km on the transmission line, respectively. The impedance trajectory of the fault loop is calculated by the proposed scheme and directly calculated by (35) (defined as scheme 1), respectively. The comparison is shown in Fig. 9. The impedance trajectory of the proposed scheme can be stable inside or outside the impedance circle to ensure the correct operation of the distance protection. However, the impedance trajectory of scheme 1 passing through the impedance circle is not sufficiently stable, which may cause incorrect operation of the distance protection. Therefore, the proposed scheme has a relatively strong ability to resist the transition resistance.

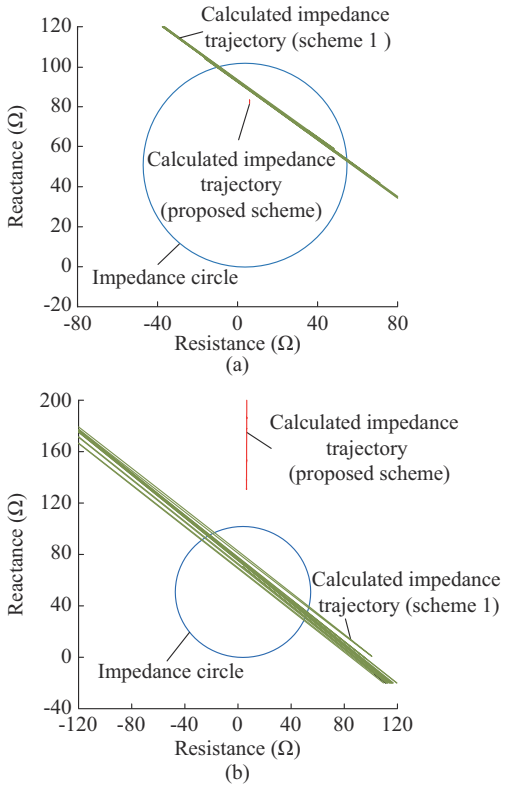

Fig. 9. Impedance trajectory of fault loop when a single-phase grounding fault with a 300 Ω transition resistance is set at 300 and 378 km on transmission line. (a) 300 km. (b) 378 km.

Taking a single-phase grounding fault as an example, more simulation examples and data for the proposed scheme are summarized in Table III. "Y" means that the calculated impedance trajectory is inside the setting impedance circle. "N" means that the calculated impedance trajectory is outside the setting impedance circle. "-" means that the calculated value of the transition resistance is less than the threshold value (300 Ω) and no impedance calculation is required. "√" indicates that the distance protection operates or does not operate correctly. "×" indicates that the distance protection fails to operate or incorrectly operates. "t" represents the time required for distance protection to make a judgement. It can be observed from the data in Table III that the proposed scheme can obtain a quick judgment in about 15 ms for all types of faults. Moreover, the proposed scheme has a strong ability to resist the transition resistance.

TABLE III
SIMULATION EXAMPLES AND DATA FOR PROPOSED SCHEME

Fault type	Fault location (km)	R_F (Ω)	x_n (km)	$R'_{F(n)}$ (Ω)	Impedance trajectory	Distance protection	t (ms)
Internal fault	100	0	100.65	0.00	-	√	13.70
		50	103.36	69.80	-	√	13.50
		100	105.96	139.66	-	√	13.40
		200	110.84	279.55	-	√	13.40
		300	110.21	419.65	Y	√	14.80
	200	0	203.71	0.00	-	√	14.50
		50	206.70	101.69	-	√	13.30
		100	209.33	203.53	-	√	13.20
		200	208.71	407.60	Y	√	14.77
		300	214.15	610.40	Y	√	14.88
	300	0	299.10	–0.03	-	√	15.65
		50	299.33	186.93	-	√	15.14
		100	301.63	301.63	Y	√	14.95
		200	308.58	746.85	Y	√	15.03
		300	316.05	1119.80	Y	√	15.12
	350	0	350.43	–0.06	-	√	16.88
		50	340.72	316.82	Y	√	15.46
		100	334.64	633.68	N	×	15.53
		200	327.04	1265.95	N	×	15.59
		300	324.90	1888.65	N	×	15.68
External fault	378	0	377.80	–0.10	-	√	12.99
		50	341.60	522.66	N	√	15.95
		100	326.60	1023.15	N	√	15.81
		200	322.19	2030.07	N	√	13.53
		300	400.64	3036.14	N	√	13.33

Owing to the weak feed-in characteristic of the wind farm, the opposite terminal source exhibits a strong feed-in function during faults. Obviously, this is similar to the case of a heavily loaded line with a strong infeed from the remote source, where the assumption that the branching coefficient C_F is a real number is no longer applicable. At this time, the calculation error caused by the above assumption is large. In order to avoid the incorrect operation of distance protection, the proposed scheme sets a threshold $R'_{F(set)}$. If the calculated R'_F exceeds $R'_{F(set)}$, the impedance trajectory is cal-

culated, and the impedance circle is introduced to identify the fault position. Therefore, in the simulation cases in Table III, the impedance trajectories exceed the impedance circle for the high-impedance faults at the end of the protection zone (e.g., at 350 km), and the proposed scheme refuses to operate. In regards to the above situation, the proposed scheme needs further research and improvement, which will be developed in the future work.

4) Effect of Noise

To simulate a real situation, white Gaussian noise is added to the sampled signal. In the case of different signal-to-noise ratios (SNRs), the proposed scheme is compared with the traditional time-domain distance protection scheme. A single-phase metallic grounding fault is set at 100 and 350 km on the transmission line as examples for comparison. The SNR is set to be 30 and 20 dB, respectively. A comparison between the proposed and traditional schemes is shown in Fig. 10. The proposed scheme is less affected by noise, and the advantages of the proposed scheme are more obvious at a smaller SNR.

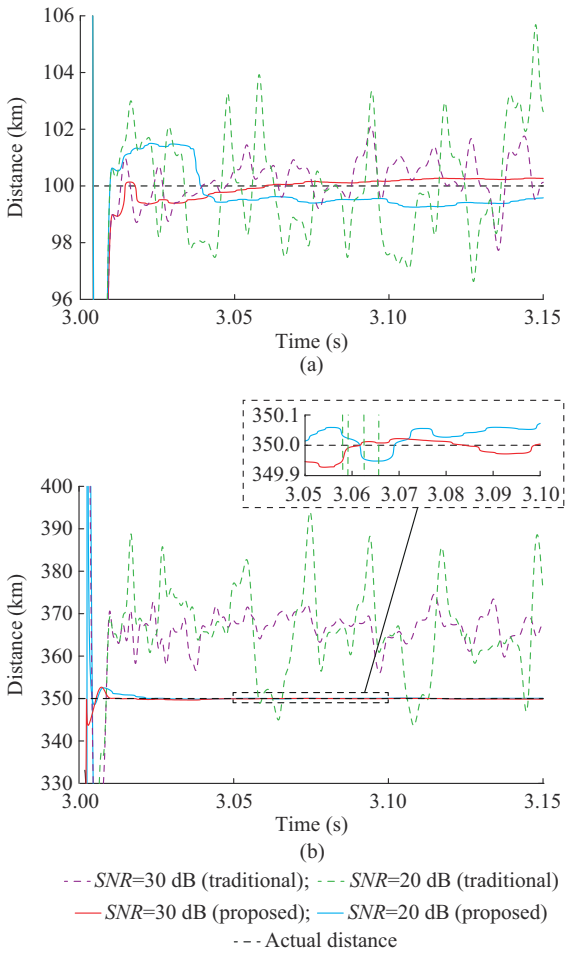

Fig. 10. Influence of noise when a single-phase metallic ground fault is set at 100 and 350 km on transmission line. (a) 100 km. (b) 350 km.

5) Performance of Proposed Scheme for Different Fault Types

The proposed scheme is also applicable to other types of faults. Line-to-line faults and three-phase-to-ground faults at 100 km on the transmission line are used as examples. The proposed scheme is compared with the traditional R-L algorithm and the Fourier algorithm. The simulation results are shown in Fig. 11. The proposed scheme still has obvious advantages. In the case of a three-phase-to-ground fault, the fault current is quite small owing to the weak feed characteristic of the wind power system, and the power frequency current accounts for a lower proportion of the fault current. The Fourier algorithm cannot correctly reflect the fault distance, while the proposed scheme is less affected.

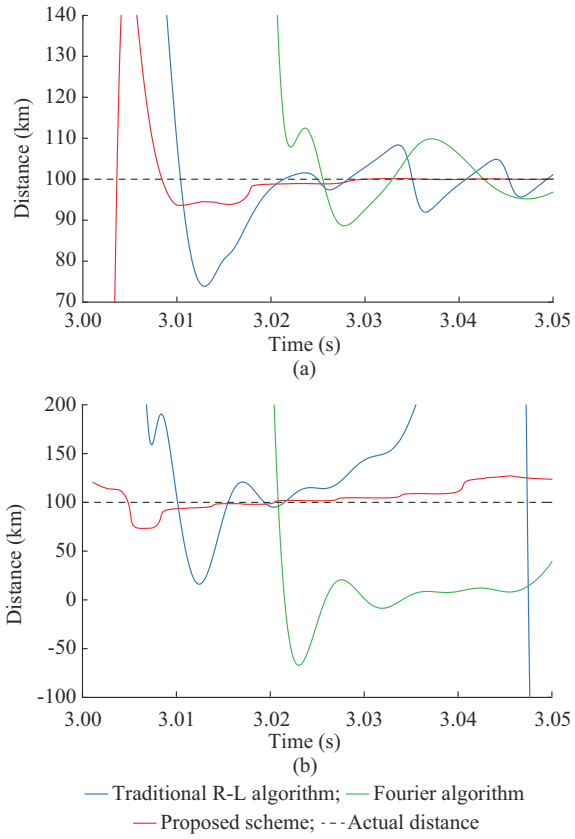

Fig. 11. Simulation results of phase-to-phase fault and three-phase fault at 100 km on transmission line. (a) Phase-to-phase fault. (b) Three-phase fault.

V. Conclusion

For the time-domain distance protection scheme used for transmission lines connected to wind farms, the location error of the R-L model caused by ignoring the distributed capacitance of the transmission line is deduced in this paper, and its influence on distance protection is analyzed. The analysis shows that the operation of distance protection may fail when ignoring the distributed capacitance of the transmission line as the system voltage level and transmission distance increase. In this paper, the precise range over which distance protection fails to operate is theoretically analyzed.

For the time-domain distance protection scheme based on the R-L model, an algorithm for improving the error weights based on a short-term data window, which converges faster than the commonly used long-term data window, is proposed in this paper, and the stability of the calculated results is significantly improved.

Further, a new scheme for time-domain distance protection that uses the Bergeron model for iteration is proposed in this paper. Compared with the traditional scheme that directly uses the R-L model, the calculation error is significantly reduced. Moreover, the calculation speed and stability and the robustness to the transition resistance are improved. Obviously, compared with the traditional time-domain distance protection scheme, the dead zone for the operation of the proposed protection scheme is much smaller. However, it is noted that the proposed scheme cannot reliably operate when a high-resistance fault occurs at the end of the line. This problem will be further studied in our future work.

REFERENCES

[1] M. I. Blanco, "The economics of wind energy," *Renewable & Sustainable Energy Reviews*, vol. 13, no. 6-7, pp. 1372-1382, Aug.-Sept. 2011.

[2] Z. Zhuo, N. Zhang, X. Xie *et al*., "Key technologies and developing challenges of power system with high proportion of renewable energy," *Automation of Electric Power Systems*, vol. 45, no. 9, pp. 171-191, Mar. 2021.

[3] P. B. Eriksen, T. Ackermann, H. Abildgaard *et al*., "System operation with high wind generation," *IEEE Power and Energy Magazine*, vol. 3, no. 6, pp. 65-74, Oct. 2005.

[4] L. Zhang, T. Ye, Y. Xin *et al.*, "Problems and measures of power grid accommodating large scale wind power," *Proceedings of the CSEE*, vol. 30, no. 25, pp. 1-9, Sept. 2010.

[5] Q. Tu, S. Miao, F. Yao *et al*., "Forecasting scenario generation for multiple wind farms considering time-series characteristics and spatial-temporal correlation," *Journal of Modern Power Systems and Clean Energy*, vol. 9, no. 4, pp. 837-848, Jul. 2021.

[6] S. Chandrasekar and R. Gokaraju, "Dynamic phasor modeling of type 3 DFIG wind generators (including SSCI phenomenon) for short-circuit calculations," *IEEE Transactions on Power Delivery*, vol. 30, no. 2, pp. 887-897, Oct. 2015.

[7] J. Morren and S. W. H. de Haan, "Ride through of wind turbines with doubly-fed induction generator during a voltage dip," *IEEE Transactions on Energy Conversion*, vol. 20, no. 2, pp. 435-441, Jun. 2005.

[8] D. F. Howard, T. G. Habetler, and R. G. Harley, "Improved sequence network model of wind turbine generators for short-circuit studies," *IEEE Transactions on Energy Conversion*, vol. 27, no. 4, pp. 968-977, Dec. 2012.

[9] E. Muljadi, N. Samaan, V. Gevorgian *et al*., "Different factors affecting short circuit behavior of a wind power plant," *IEEE Transactions on Industry Applications*, vol. 49, no. 1, pp. 284-292, Jan.-Feb. 2013.

[10] S. A. Saleh, A. S. Aljankawey, R. Meng *et al*., "Impacts of grounding configurations on responses of ground protective relays for DFIG-based WECSs–Part I: solid ground faults," *IEEE Transactions on Industry Applications*, vol. 51, no. 4, pp. 2804-2818, Jul.-Aug. 2015.

[11] S. A. Saleh, A. S. Aljankawey, R. Meng *et al*., "Impacts of grounding configurations on responses of ground protective relays for DFIG-based WECSs–Part II: high-impedance ground faults," in *Proceedings of 2015 IEEE/IAS 51st Industrial & Commercial Power Systems Technical Conference (I&CPS)*, Calgary, Canada, Sept. 2015, pp. 1-9.

[12] Y. Zheng, T. Wu, F. Hong *et al*., "Transmission line distance protection under current transformer saturation," *Journal of Modern Power Systems and Clean Energy*, vol. 9, no. 1, pp. 68-76, Jan. 2021.

[13] S. Maihemuti, W. Wang, H. Wang *et al*., "Voltage security operation region calculation based on improved particle swarm optimization and recursive least square hybrid algorithm," *Journal of Modern Power Systems and Clean Energy*, vol. 9, no. 1, pp. 138-147, Jan. 2021.

[14] C. Zhou, Z. Wang, P. Ju *et al*., "High-voltage ride through strategy for DFIG considering converter blocking of HVDC system," *Journal of Modern Power Systems and Clean Energy*, vol. 8, no. 3, pp. 491-498, May 2020.

[15] K. Jia, Y. Li, Y. Fang *et al*., "Transient current similarity based protection for wind farm transmission lines," *Applied Energy*, vol. 225, pp. 52-59, May 2018.

[16] B. Li, J. Liu, X. Wang *et al*., "Fault studies and distance protection of transmission lines connected to DFIG-based wind farms," *Applied Sciences*, vol. 8, no. 4, pp. 562, Apr. 2018.

[17] A. Han, Z. Zhang, X. Yin *et al.*, "Research on fault characteristic and grid connecting-point protection scheme for wind power generation with doubly-fed induction generator," *Transactions of China Electrotechnical Society*, vol. 27, no. 4, pp. 233-239, Apr. 2012.

[18] A. K. Pradhan and G. Joos, "Adaptive distance relay setting for lines connecting wind farms," *IEEE Transactions on Energy Conversion*, vol. 22, no. 1, pp. 206-213, Mar. 2007.

[19] A. Hooshyar, M. A. Azzouz, and E. F. El-Saadany, "Distance protection of lines connected to induction generator-based wind farms during balanced faults," *IEEE Transactions on Sustainable Energy*, vol. 5, no. 4, pp. 1193-1203, Oct. 2014.

[20] H. Zhang, W. Wang, L. Zhu *et al*., "An adaptive setting method for distance protection of transmission lines connecting wind farms," *Power System Technology*, vol. 33, no. 3, pp. 89-93, Feb. 2009.

[21] H. Sadegh, "A novel method for adaptive distance protection of transmission line connected to wind farms," *International Journal of Electrical Power & Energy Systems*, vol. 43, no. 1, pp. 1376-1382, Apr. 2012.

[22] T. Wang, F. Li, and S. He, "Factors impacting distance protection for tie line of wind farm and corresponding countermeasures," *Power System Technology*, vol. 38, no. 5, pp. 1420-1424, May 2014.

[23] C. Su，F. Li, and Y. Wu, "An analysis on short-circuit characteristic of wind turbine driven doubly fed induction generator and its impact on relay setting," *Automation of Electric Power Systems*, vol. 35, no. 6, pp. 86-91, Mar. 2011.

[24] M. Khoddam and H. K. Karegar, "Effect of wind turbines equipped with doubly-fed induction generators on distance protection," in *Proceedings of 2011 International Conference on Advanced Power System Automation and Protection*, Beijing, China, Oct. 2011, pp. 1349-1353.

[25] A. Hooshyar, M. A. Azzouz, and E. F. El-Saadany, "Distance protection of lines emanating from full-scale converter-interfaced renewable energy power plants–Part I: problem statement," *IEEE Transactions on Power Delivery*, vol. 30, no. 4, pp. 1770-1780, Aug. 2015.

[26] S. de Rijcke, P. S. Pérez, and J. Driesen, "Impact of wind turbines equipped with doubly-fed induction generators on distance relaying," in *Proceedings of IEEE PES General Meeting*, Minneapolis, USA, Jul. 2010, pp. 1-10.

[27] L. Chen, J. Zhang, J. Du *et al*., "Applicability of phase-comparison distance protection based on polarized voltage for outgoing transmission line of DFIG-based wind farm," *Electric Power Automation Equipment*, vol. 36, no. 9, pp. 74-79, Sept. 2016.

[28] B. Zhang, J. Zhang, B. Yuan *et al*., "Impact of wind farm integration on relay protection (6): analysis of distance protection for wind farm outgoing transmission line," *Electric Power Automation Equipment*, vol. 33, no. 6, pp. 1-6, Jun. 2013.

[29] Z. Yang, X. Kong, L. Wang *et al*., "Distance protection scheme for interconnection line of doubly-fed induction generator based wind farm," *Transactions of China Electrotechnical Society*, vol. 31, no. 24, pp. 252-260, Dec. 2016.

[30] Y. Fan, J. Hou, Q. Yao *et al*., "Time-domain equation model deviation correction distance protection for cluster wind power transmission line with anti-transient ability," *Electric Power Automation Equipment*, vol. 38, no. 1, pp. 10-18, Jan. 2018.

[31] Y. Chen, M. Wen, X. Yin *et al.*, "Distance protection for transmission lines of DFIG-based wind power integration system," *International Journal of Electrical Power & Energy Systems*, vol. 100, pp. 438-448, Sept. 2018.

[32] Y. Fan and J. Hou, "Time domain distance protection for long distance outgoing line of wind power system based on distributed parameter model," *Power System Protection and Control*, vol. 46, no. 19, pp. 26-33, Oct. 2018.

[33] Q. Yang, "Microprocessor based distance protection," Ph.D. dissertation, Department of Electrical Engineering and Computer Science, University of New South Wales, Sydney, Australia, 1981.

[34] X. Kong, Z. Zhang, X. Yin *et al*., "Study of fault current characteristics of the DFIG considering dynamic response of the RSC," *IEEE Transactions on Energy Conversion*, vol. 29, no. 2, pp. 278-287, Jun. 2014.

[35] J. Ouyang and X. Xiong, "Dynamic behavior of the excitation circuit of a doubly-fed induction generator under a symmetrical voltage drop," *Renewable Energy*, vol. 71, pp. 629-638, Nov. 2014.

[36] B. LI, J. He, W. Chang *et al*., "Bergeron model based distance protection for long transmission lines," *Automation of Electric Power Systems*, vol. 34, no. 23, pp. 52-56, Dec. 2010.

Zepeng Hu received the B.S. degree in electrical engineering from Chongqing University, Chongqing, China, in 2019. He is now a Graduate Student studying at Tianjin University, Tianjin, China. His research interests include

protection and control of power systems.

Bin Li received the B.S., M.S., and Ph.D. degrees in electrical engineering from Tianjin University, Tianjin, China, in 1999, 2002, and 2005, respectively. He was an Academic Visitor with the University of Manchester, Manchester, UK, in 2006. From 2008 to 2009, he worked in the design and application of protection relays with AREVA, London, UK. Currently, he is a Professor with the School of Electrical Engineering and Automation, Tianjin University. His research interests include protection and control of power systems.

Yuping Zheng received the B.S. degree from Hefei University of Technology, Hefei, China, in 1983, the M.S. degree from Nanjing Automation Research Institute, Nanjing, China, in 1986, and the Ph.D. degree from Wuhan University, Wuhan, China, in 2004. Currently, he is working in the State Key Laboratory of Smart Grid Protection and Control, NARI Group Corporation, Nanjing, China. His research interests include relay protection and control of AC/DC hybrid power system.

Tonghua Wu received the B.S. degree from Hefei University of Technology, Hefei, China, in 1999, the M.S. degree from State Grid Electric Power Research Institute, Nanjing, China, in 2005. Currently, he is pursuing the Ph.D. degree of automation of electric power systems in Hohai University, Nanjing, China. His interests include relay protection and control of AC/DC hybrid power system.

Jiawei He received the B.S, M.S., and Ph.D. degrees in electrical engineering from Tianjin University, Tianjin, China, in 2014, 2017, and 2021, respectively. Currently, he is working as a Postdoctor in Tianjin University. His research interests include protection and control of DC grid, and protection and control of power system with high proportion of renewable energy.

Bin Yao received the B.S. and M.S. degrees in electrical engineering from Tianjin University, Tianjin, China, in 2000 and 2003, respectively. Currently, he is working in the School of Electrical Engineering and Automation, Tianjin University. His research interests include fault analysis and relay protection of power systems.

Yaru Sheng received the B.S. degree in electrical engineering from China University of Mining and Technology, Beijing, China, in 2016, and the M.S. degree in electrical engineering from Shandong University, Jinan, China, in 2019. She is now a Ph.D. student studying at Tianjin University, Tianjin, China. Her research interests include protection and control of power systems.

Wei Dai received the B.S. degree from Huazhong University of Science and Technology, Wuhan, China, in 2004, and the M.S. degree from Southeast University, Nanjing, China, in 2006. He is currently working in the State Key Laboratory of Smart Grid Protection and Control, NARI Group Corporation, Nanjing, China. His research interests include relay protection of AC/DC hybrid power system and DC system.

Xindong Li received the B.S. and M.S. degrees from Huazhong University of Science and Technology, Wuhan, China, in 2004 and 2007, respectively. He is currently working in the State Key Laboratory of Smart Grid Protection and Control, NARI Group Corporation, Nanjing, China. His research interests include relay protection and control of AC/DC hybrid power system.